PCCP

RSC Publishing

PAPER

View Article Online
View Journal | View Issue

Cite this: *Phys. Chem. Chem. Phys.*, 2013, **15**, 7785

DFT based study of transition metal nano-clusters for electrochemical NH_3 production†

J. G. Howalt,[ab] T. Bligaard,[bcd] J. Rossmeisl[b] and T. Vegge*[ac]

Received 21st December 2012,
Accepted 26th March 2013

DOI: 10.1039/c3cp44641g

www.rsc.org/pccp

Theoretical studies of the possibility of producing ammonia electrochemically at ambient temperature and pressure without direct N_2 dissociation are presented. Density functional theory calculations were used in combination with the computational standard hydrogen electrode to calculate the free energy profile for the reduction of N_2 admolecules and N adatoms on transition metal nanoclusters in contact with an acidic electrolyte. This work has established linear scaling relations for the *dissociative* reaction intermediates NH, NH_2, and NH_3. In addition, linear scaling relations for the *associative* reaction intermediates N_2H, N_2H_2, and N_2H_3 have been determined. Furthermore, correlations between the adsorption energies of N, N_2, and H have been established. These scaling relations and the free energy corrections are used to establish volcanoes describing the onset potential for electrochemical ammonia production and hence describe the potential determining steps for the electrochemical ammonia production. The competing hydrogen evolution reaction has also been analyzed for comparison.

I. Introduction

In the past decade, it has become more apparent than ever that mankind needs to move towards more sustainable energy consumption with significantly smaller carbon footprint per capita.

There are a number of possible ways that could potentially be used to reduce the global carbon footprint and a number of technologies have already been implemented to generate electrical power more or less sustainably, such as, for example, wind turbines, solar cells, biomass fired power plants, *etc.* With time, and with increasing prices of fossil resources, some of these may become economically competitive with fossil resources. A difficult problem to address is that of substituting transportation fuels. To make sustainable transportation fuels economically, one needs not only a competitively inexpensive way to harvest a sustainable source of energy, but also to store the energy in a convenient form with a high enough volumetric and gravimetric energy density, and in a form that can easily be transferred to a vehicle. Since catalysis can facilitate the efficient synthesis of chemicals with high energy contents, catalysis plays a key role in many of the potential scenarios for reducing our dependence on fossil resources.

One chemical compound of great versatility is ammonia. Ammonia is primarily used for making fertilizers, ultimately sustaining roughly one-third of the world's population.[1,2] In terms of reducing the carbon footprint, ammonia is interesting for a number of reasons. First, there is potential for improving the sustainability of the already huge industrial catalytic production of ammonia, which is on the order of over 100 million metric tons annually, and responsible for 1–2% of the global energy consumption. Secondly, ammonia is becoming increasingly interesting as a potential transportation fuel.[3] As an energy carrier, ammonia has the benefit that it can be used in the very energy efficient fuel cells such as the solid oxide fuel cell (SOFC) or a direct ammonia fuel cell (DAFC). Furthermore, it has the interesting feature of not emitting CO_2 while having a high energy density that is comparable with traditional fossil fuels, both volumetrically and gravimetrically.[3,4] A highly energy-efficient method for the synthesis of ammonia (NH_3) from molecular nitrogen (N_2) in air is therefore desirable. Currently, ammonia synthesis is achieved by the Haber–Bosch process that initially dissociates the N_2 bond and then protonates each nitrogen atom.[5] This is the *dissociative mechanism*. In contrast, the natural enzymatic process in nitrogenase takes place by initially weakening the N–N bond through successive protonations until the dissociation barrier is low enough that

[a] *Department of Energy Conversion and Storage, Technical University of Denmark, DK-4000 Roskilde, Denmark. E-mail: teve@dtu.dk*
[b] *Center for Atomic-scale Materials Design, Department of Physics, Technical University of Denmark, DK-2800 Kgs., Lyngby, Denmark*
[c] *SUNCAT Center for Interface Science and Catalysis, SLAC National Accelerator Laboratory, 2575 Sand Hill Road, Menlo Park, CA 94025, USA*
[d] *Department of Chemical Engineering, Stanford University, Stanford, CA 94305, USA*

† Electronic supplementary information (ESI) available. See DOI: 10.1039/c3cp44641g

the N–N bond breaks; this process is referred to as the *associative mechanism*.[6] The Haber–Bosch process is energy-intensive and centralized due to the high required temperature and pressure and it is associated with a high capital cost to construct the production plants. What we aim for is the electricity-based production of ammonia utilizing electrochemistry, thus allowing small production scales and the use of renewable energy sources like windmills or solar cells.

In the past several years, numerous experimental[7–21] and theoretical[22–34] studies have examined ammonia synthesis and they offer excellent insight into the challenges faced when developing new catalytic materials for this reaction. It has been shown in previous studies that ammonia synthesis is very structure sensitive on metal surfaces and primarily occurs on the surface steps of Fe and Ru[22,35,36] and one could expect the associative mechanism to be even more structure sensitive. The competing hydrogen evolution reaction (HER) is structure insensitive[37] and we have therefore looked at highly under-coordinated nanoclusters as a way to investigate this discrepancy.

Furthermore, it has been shown that a similar reaction, CO oxidation, can be performed on transition metal nanoparticles consisting of more noble metals at lower temperature[36,40] than traditionally-used catalysts for this reaction. On the basis of the development of density functional theory (DFT), it has become feasible to reliably model chemical reactions.[41] We have used DFT calculations to investigate electrocatalytic production of ammonia. In this work we have studied ammonia synthesis on the highly under-coordinated M12 nanoclusters, see Fig. 1, and hence the extreme domain of possible under-coordination that can be achieved, which earlier has been shown to dramatically change the reactivity of inert metals,[34,38,39] and compare the nanocluster to the traditionally studied fcc(211) surfaces. While previous studies have looked at stepped metal surfaces, the B5 sites in particular,[22,31] we perform all calculations on a consistent calculational basis, so we can directly compare results for the M12 nanocluster with the reference system of a fcc(211) stepped surface. We have investigated the reaction intermediates for the dissociative and associative mechanisms on fcc(211) surfaces and M12 nanoclusters for a large number of transition metals and developed scaling relations similar to stepped and close-packed metal surfaces. Based on vibrational calculations, entropy and zero point energy corrections calculated using statistical mechanics we construct Gibbs free energy diagrams for both reaction pathways. These diagrams can then be used to determine the lowest potential which will make each part reaction exothermic, this is then defined as the onset potential for the overall reaction and can be used to construct volcano plots visualizing the onset potential for the electrochemical ammonia production across the investigated metals.

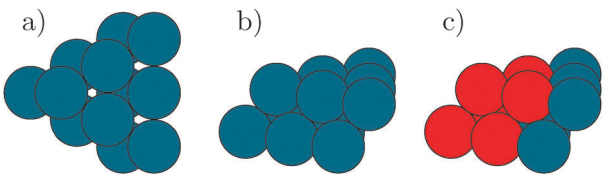

Fig. 1 (a) The M12 nanocluster seen from above. The close-packed structure is shown and the layers arranged as two fcc close-packed layers would be in a normal fcc structure. (b) The M12 nanocluster seen from the side. (c) The front six atoms are the ones with which the intermediates are allowed to bind.

II. Computational method

A. The M12 cluster

The model system we analyze is the M12 nanocluster, which contains 12 metal atoms and has previously served as a model for an under-coordinated and very small nanoparticle.[40] The atoms in the M12 are positioned in two layers, with each layer containing six atoms. Each layer follows the fcc close-packed surface structure creating a triangle, see Fig. 1a. The layers are placed above each other in the same fashion as they would in a normal close-packed slab, see Fig. 1b. For the M12 nanocluster two lattice constants were used for each of the investigated metals. The first lattice constant was determined from calculations of the bulk lattice constants in the fcc structure for each metal (denoted bulk M12). The second lattice constant was determined by allowing the M12 nanocluster to relax the lattice constant until the lowest energy configuration was found (denoted relaxed M12). For both types of M12 nanoclusters the structure was kept fixed during all adsorption calculations of reaction species.

In this study, the analysis was limited to the adsorption sites indicated by the atoms marked with red in Fig. 1c for the reaction intermediates, presented in eqn (3c)–(3h) and (4b)–(4g). These sites are chosen because they are highly under-coordinated and have other features than those of the back side of the clusters which resembles a step closer, but lack the stabilizing terraces and have been analyzed in great detail in ref. 34.

B. DFT calculations

The calculations were carried out with DFT[42,43] using the RPBE exchange correlation functional[44] in the projector augmented wave method[45,46] as implemented in the GPAW code.[47–49] A grid of (3,3) for the finite difference stencils has been used together with a grid spacing of 0.18 Å, at least 20 free bands above the Fermi level, and a Monkhorst–Pack[50] *k*-point sampling of the $2 \times 2 \times 2$. A 7 Å vacuum layer around the nanocluster has been applied. In solving the electronic density self-consistently, the convergence criteria have been chosen such that the changes in energy were $<10^{-5}$ eV and the density was 0.0001 electrons per valence electron and for most systems chosen orders of magnitude lower. Spin polarized calculations were also performed for metals that usually have a magnetic moment, such as Fe, Ni and Co although the magnetic moment could depend on the fixed geometry. In all calculations a Fermi smearing of 0.0001 eV has been used. The atomic simulation environment ASE[51] was used to set up the atomic structure of these systems. All relaxations of the adsorbates (N, H, NH, *etc.*) sitting on the bulk M12 nanocluster were carried out using the BFGS optimizer within ASE.

For the reference calculations on the fcc(211) stepped surface, a slab with five layers was utilized and in the direction following the edge of the step it was repeated once such that

each layer consisted of 3 × 2 atoms. Of the five layers that were employed, the top two were allowed to relax and a vacuum of 7 Å on both sides of the slab was used. The utilized computational criteria only differ from the clusters in that a Monkhorst–Pack *k*-point sampling of 4 × 4 × 1 was used, and the Fermi smearing was 0.0001 eV.

C. Reaction pathways

In the process of forming ammonia electrochemically, it is convenient to model the anode reaction

$$H_2 \rightleftharpoons 2H^+ + 2e^- \quad (1)$$

as the source of electrons and protons. The electrons are transported to the cathode side through an external circuit, while the protons are introduced into the proton conducting electrolyte and sustain the equilibrium and diffuse to the cathode. At the cathode a nitrogen molecule will react with the protons and electrons in the following overall reaction

$$N_2 + 6H^+ + 6e^- \rightarrow 2NH_3, \quad (2)$$

to form ammonia at the catalytically active site.

In this study two pathways to form ammonia have been investigated, the Heyrovski-type[52] reaction for both the associative and dissociative mechanisms. For the Heyrovski-type mechanism, the adsorbed species of NH_x or N_2H_x (x = {0,1,2,3}) are directly protonated, in the following way: the proton directly attaches to the molecule from the electrolyte and the electron comes from the surface and merges with the proton to create a hydrogen bonded to the molecule. In principle, the Tafel-type reaction could also occur, but this requires the reaction barriers for the hydrogenation steps[34,53] to be overcome, and will therefore require a higher temperature to drive the process forward. This is due to the fact that the Tafel reaction[54] requires the proton and the electron to merge to form a hydrogen adatom on the surface first, which then reacts with the adsorbed species of NH_x or N_2H_x (x = {0,1,2,3}). These reaction barriers have not be investigated in the present work.

The Heyrovski-type reactions for the electrochemical ammonia formation are presented below. First, we consider the dissociative Heyrovsky mechanism where the nitrogen molecule is dissociated on the surface and then subsequently protonated (an asterisk, *, denotes a surface site):

$$N_2(g) + 6(H^+ + e^-) + 2^* \rightleftharpoons N_2{}^{**} + 6(H^+ + e^-) \quad (3a)$$

$$N_2{}^{**} + 6(H^+ + e^-) \rightleftharpoons 2N^* + 6(H^+ + e^-) \quad (3b)$$

$$2N^* + 6(H^+ + e^-) \rightleftharpoons NH^* + N^* + 5(H^+ + e^-) \quad (3c)$$

$$NH^* + N^* + 5(H^+ + e^-) \rightleftharpoons NH_2{}^* + N^* + 4(H^+ + e^-) \quad (3d)$$

$$NH_2{}^* + N^* + 4(H^+ + e^-) \rightleftharpoons NH_3{}^* + N^* + 3(H^+ + e^-) \quad (3e)$$

$$NH_3{}^* + N^* + 3(H^+ + e^-) \rightleftharpoons NH_3{}^* + NH^* + 2(H^+ + e^-) \quad (3f)$$

$$NH_3{}^* + NH^* + 2(H^+ + e^-) \rightleftharpoons NH_3{}^* + NH_2{}^* + (H^+ + e^-) \quad (3g)$$

$$NH_3{}^* + NH_2{}^* + (H^+ + e^-) \rightleftharpoons 2NH_3{}^* \quad (3h)$$

$$2NH_3{}^* \rightleftharpoons NH_3{}^* + NH_3(g) + * \quad (3i)$$

$$NH_3(g) + NH_3{}^* + * \rightleftharpoons 2NH_3(g) + 2^* \quad (3j)$$

Secondly, the associative Heyrovski mechanism is considered, where the nitrogen molecule attaches to the surface and is protonated before the nitrogen–nitrogen bond dissociates. In the equations below, information from the calculations has been used, where the addition of the fourth H to the molecule $N_2H_3{}^*$ weakens the N–N bond so much that the molecule readily dissociates into NH_x species on the surface.

$$N_2(g) + 6(H^+ + e^-) + 2^* \rightleftharpoons N_2{}^{**} + 6(H^+ + e^-) \quad (4a)$$

$$N_2{}^{**} + 6(H^+ + e^-) \rightleftharpoons N_2H^{**} + 5(H^+ + e^-) \quad (4b)$$

$$N_2H^{**} + 5(H^+ + e^-) \rightleftharpoons N_2H_2{}^{**} + 4(H^+ + e^-) \quad (4c)$$

$$N_2H_2{}^{**} + 4(H^+ + e^-) \rightleftharpoons N_2H_3{}^{**} + 3(H^+ + e^-) \quad (4d)$$

$$N_2H_3{}^{**} + 3(H^+ + e^-) \rightleftharpoons NH_2{}^* + NH_2{}^* + 2(H^+ + e^-) \quad (4e)$$

$$NH_2{}^* + NH_2{}^* + 2(H^+ + e^-) \rightleftharpoons NH_3{}^* + NH_2{}^* + (H^+ + e^-) \quad (4f)$$

$$NH_3{}^* + NH_2{}^* + (H^+ + e^-) \rightleftharpoons 2NH_3{}^* \quad (4g)$$

$$2NH_3{}^* \rightleftharpoons NH_3{}^* + NH_3(g) + * \quad (4h)$$

$$NH_3{}^* + NH_3(g) + * \rightleftharpoons 2NH_3(g) + 2^* \quad (4i)$$

Alternatively, reaction (4d) has the possibility of splitting into NH and NH_2 on the surface and has been observed on some of the metals.

D. Electrochemical modelling

With DFT it is possible to calculate the reaction energy, ΔE, for each of the reaction intermediates described above in the dissociative and associative Heyrovski pathways. This reaction energy is calculated with respect to the gas-phase molecules of hydrogen and nitrogen and a clean M12 nanocluster:

$$\Delta E = E_{M_{12}-N_xH_y{}^*} - \left(E_{M_{12}} + \frac{x}{2}E_{N_2(g)} + \frac{y}{2}E_{H_2(g)}\right), \quad (5)$$

where $E_{M_{12}+N_xH_y}$ is the total energy of the system containing the M12 nanocluster with the adsorbed N_xH_y species, E_{M12} is the total energy of the system containing only the M12 nanocluster, while $E_{N_2(g)}$ and $E_{H_2(g)}$ are the calculated gas-phase energies of nitrogen and hydrogen molecules, respectively.

The reaction energies give information about the catalytic properties for ammonia formation, which we shall elaborate further upon in the discussion of the scaling relations in one of the later sections. However, for a thorough understanding, free energy corrections for each reaction intermediate need to be determined and included in the analysis.

We obtain a reasonable approximation to the free energy from the DFT calculations for the adsorbate relative to the gas-phase molecular nitrogen and hydrogen from the expression:

$$\Delta G = \Delta E + \Delta E_{ZPE} - T\Delta S, \quad (6)$$

where the ΔE_{ZPE} and ΔS are the reaction zero point energy and reaction entropy, respectively, and we have ignored thermal internal energy contributions.

Within the harmonic approximation, it is possible to calculate the vibrational frequencies for all reaction intermediates

using a finite difference method.[55] The surface species were only allowed to vibrate, while the surface atoms were kept fixed and hence the change in free energy of the metal atoms was neglected. From the vibrational frequencies the zero point energy and the entropy under the reaction conditions can be determined. The zero point energy term is given as

$$E_{\mathrm{ZPE}} = \sum_i \frac{1}{2} h\nu_i. \quad (7)$$

The vibrational entropy contribution was calculated explicitly using standard equations from statistical mechanics and is shown below:

$$S_{\mathrm{vib}} = R\sum_i \left(\frac{\Theta_{\mathrm{vi}}/T}{\exp\left(\frac{\Theta_{\mathrm{vi}}}{T}\right) - 1} - \ln\left[1 - \exp\left(\frac{-\Theta_{\mathrm{vi}}}{T}\right)\right] \right). \quad (8)$$

In this expression, the characteristic vibrational temperature, Θ_{vi}, is equal to $h\nu_i/k_B$. Here R is the gas constant, h is Planck's constant, k_B is Boltzmann's constant and T is the absolute temperature and ν is the vibrational frequency.

In addition to the entropy and zero point energy corrections we include the effects of the applied potential driving the electrochemical reaction. To include the effect of potential, we use the computational standard hydrogen electrode,[56] which has been successfully applied to describe a number of electrochemical reactions, including the trends in oxygen[57,58] and nitrogen[35] and CO_2 reduction.[59] The procedure of the computational standard hydrogen electrode is briefly outlined below.[56]

The standard hydrogen electrode (SHE) has been chosen as reference potential. The chemical potential (the free energy per H) of $(H^+ + e^-)$ is related to that of $\frac{1}{2}H_2(g)$, see eqn (1). For pH = 0, a potential of $U = 0$ V relative to the SHE and a partial pressure of 1 bar of H_2 in the gas phase at 298 K, the reaction free energy of eqn (1) is equal to the net reaction of eqn (2) at an electrode.

The free energy for the reaction intermediates as defined in eqn (6) was used.

The next step is to incorporate the effects of an applied potential in all reactions involving an electron transfer and for the protons the pH. The free energy shift for a reaction involving n electrons is $-neU$ and hence the free energy reads

$$\Delta G = \Delta E + \Delta E_{\mathrm{ZPE}} - T\Delta S - neU, \quad (9)$$

This holds true for a pH value of 0.

For pH values different from 0, the correction to the free energy of H^+-ions has to be performed for the concentration dependence of the entropy, the shift reads $G(\mathrm{pH}) = -kT\ln[H^+] = kT\mathrm{pH}\ln[10]$.

All calculations presented in the present study are for a pH value of 0.

III. Results and discussion

In this section, we present the adsorption sites for the reaction intermediates, show the corresponding adsorption energies defined in eqn (5) plotted as linear scaling relations (a linear relation between different reaction intermediates) for this geometric structure, and introduce the corrections to the free energy. With these tools, the construction of volcano plots shows the onset potential for each of the reaction mechanisms when electrochemical N_2 fixation is possible.

A. Adsorption sites

We will use adsorption on the ruthenium M12 nanocluster as an illustration because the adsorption sites for this metal resemble the characteristics of all the metals studied here. Among the studied metals, from the very reactive metals such as Sc, Ti, and Nb to the very noble metals such as Au, Ag, and Cu, there are small variations in the adsorption sites. However, the M12 nanocluster has many similar types of adsorption sites, which can be divided into the usual adsorption-site subgroups such as hollow, bridge, ontop. Each of the adsorption sites in each subgroup will be slightly geometrically different and hence for each of the metals the specific electronic properties will diversify which of the specific sites are most stable. But the type of sites is close to identical throughout the investigated metals across all reaction intermediates. In Fig. 2, the adsorption sites on the ruthenium M12 nanocluster can be seen.

In Fig. 2(1) the adsorption site for N_2 is shown. The nitrogen molecule prefers to bind in a disigma type bond to the surface where the nitrogen atoms are bonded to two different metal atoms on the surface. Here the most stable sites were edges. For some sites on most of the metals, bonding of the N_2 molecule

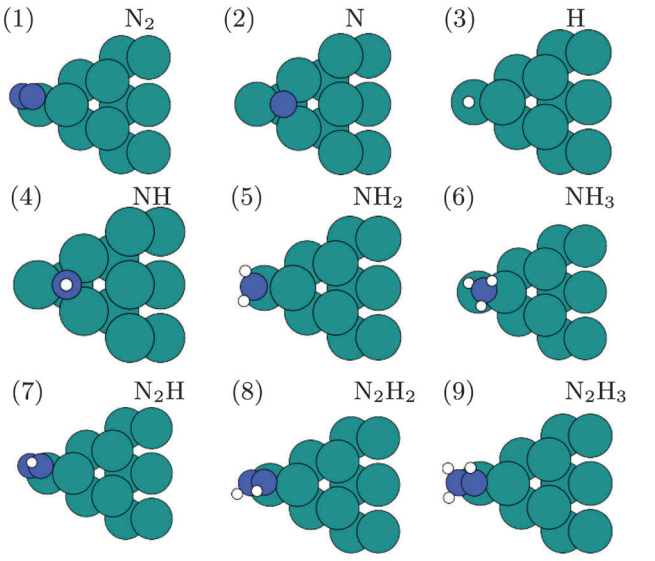

Fig. 2 The most stable adsorption sites for the reaction intermediates in both the dissociative and associative mechanisms on the ruthenium M12 nanocluster. The dark atoms are nitrogen, the small atoms are hydrogen and the light atoms are ruthenium. The adsorption sites for the adsorbates presented for the M12 nanocluster are only representative of the type of adsorption site (hollow, bridge, ontop) and not the actual bonding site for the other metals, which means a N atom could bind more strongly to another hollow site on a different metal studied in this work.

vertically to the surface was possible, where one atom was attached to the surface while the other atom was away from the surface acting as an antenna. The difference in adsorption energy between these two types of bonds is on the order of 0.1 to 0.3 eV. It should be noted that for the very reactive metals, the N_2 molecule had very few stable adsorption configurations since the splitting of the N–N bond and creation of two N* on the surface is exothermic. Furthermore, the barrier for this splitting is in the literature shown to be very low compared to the noble metals.[60]

The nitrogen adatom adsorbs on a hollow site. For hydrogen, the H_2 molecule was very rarely stable on the surface and would split into two hydrogen adatoms on the surface. The hydrogen bonding site is shown here to be a bridge site, but the difference in energy between the different types of adsorption sites was very small. NH, NH_2 and NH_3 bind to hollow, bridge and ontop sites, respectively, see Fig. 2(4–6).

The N_2H_x species on the M12 nanoclusters prefer to bond to a bridge site, where each N atom is bonded to a different metal atom, similarily to a di-sigma bonding. The configuration changes slightly depending on the number of hydrogen atoms in the surface species. Looking carefully at the figures of the N_2H_x, in Fig. 2(7–9), it is possible to see an increase in the internal bonding length as the number of hydrogen is increased and that one of the nitrogen atoms is further away from the metal atom than the other nitrogen atom. This represents the internal weakening of the N–N bond and is a key factor in the associative mechanism and the weakening of the bond between the metal and nitrogen atom. The molecule is therefore mostly bonded through one of the nitrogen atoms.

B. Scaling relations

In earlier studies it has been shown that for hydrogen containing adsorption species (such as NH_x, OH_x, CH_x, and SH_x) linear scaling relations exist that describe the adsorption energies for all species adsorbed onto either a closed packed or a stepped surface.[61] This means that the adsorption energies of AH_x (A being one of the backbone parts mentioned earlier, C, N, O, or S) on a given number of metals scale with the corresponding adsorption energy of A adsorbed onto the surface:

$$\Delta E_{AH_x} = \alpha(x)\Delta E_A + \kappa(x). \quad (10)$$

Here $\alpha(x)$ is the slope of the scaling relation, while $\kappa(x)$ is a constant. In previous studies, $\kappa(x)$ was the factor influenced by the geometric structure (whether it is a closed-packed, a stepped or another kind of surface) while the slope $\alpha(x)$ was found to be close to a constant for different surface types.

The slope is to a large extent dependent on the adsorbates number of hydrogen *versus* the maximum number of possible hydrogen in AH_x (it is 3 for NH_3).[61] The dependency on the hydrogen is such that:

$$\alpha(x) = \frac{x_{max} - x}{x_{max}}, \quad (11)$$

where x_{max} is the maximum number of hydrogen that can bond to the central atom, *i.e.* 3 for N, while the valency is defined as $(x_{max} - x)$. It should be noted that these relations exist (but vary) for different vicinal surfaces/adsorption sites. The relations are therefore useful for understanding the basic underlying trends, but one should keep in mind the complexity arising from variations in adsorption sites.

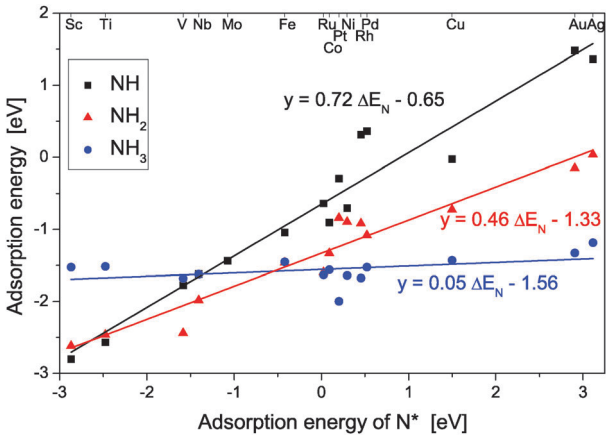

Fig. 3 The scaling relations for NH_x species on the relaxed M12 nanoclusters consisting of transition metals. The adsorption geometries are chosen as the most stable calculated ones.

In Fig. 3 the adsorption energy for NH, NH_2 and NH_3 is plotted as a function of the adsorption energy of N adatoms on the relaxed M12 nanocluster. There exist a linear relation for all NH_x species on this very under-coordinated structure. The slopes follow to a large extent the predicted ones from eqn (11). For NH, NH_2, and NH_3 the slopes are 0.72, 0.46, and 0.05. For both the bulk M12 and the relaxed M12 nanoclusters and the stepped surface fcc(211) the trend for the slope is the same, see Fig. S1–S4 in the ESI,† and the scaling relation holds true for both lattice constants. The only difference is an electronic effect that shifts the binding energy of a metal with the bulk lattice constant along the line to the adsorption energy of the metal with the relaxed lattice constant. The adsorption energies for the reaction species show that the bulk lattice constant M12 nanocluster structure is more reactive than the relaxed M12 nanocluster. This is to be expected due to the effects of stress and strain that have been shown preciously by Nørskov *et al.*[62] The values of the slopes are in good agreement with what we would have expected from the results obtained in earlier studies of the scaling relations for these species on close-packed and stepped surfaces. We cannot directly compare these calculated scaling relations with the previous described relations of NH_x species, since the underlying computational *ab initio* codes are different. Therefore, reference calculations of similar relations for a lower number of stepped fcc(211) surfaces have been carried out and the slopes $\alpha(x)$ and the constants $\kappa(x)$ are presented in Table 1. The variations in the constants between the two systems are very small and close to the uncertainty of DFT calculations. It is therefore not possible to define a noticeably geometrical effect when going from the stepped fcc(211) surface to this highly under-coordinated surface. However, the electronic effect (which is the movement down the line) is somewhat more noticeable, in the order of

Table 1 The energy scaling relations for all reaction intermediates for ammonia synthesis on the M12 nanocluster for both relax and bulk lattice constant structures and compared with the fcc(211) stepped surface. The energy relation with respect to an adsorbed N. It has to be noted that the number of metals in this study is not as large as on the M12 nanocluster calculations. The figures of the scaling relations for stepped surfaces can be found in the ESI

	fcc(211)		M12	
Adsorbate	$\alpha(y,x)$	κ (eV)	$\alpha(y,x)$	κ (eV)
N_2	0.31	−0.47	0.26	0.60
H	0.23	−0.49	0.2	−0.48
NH	0.65	−0.47	0.72	−0.65
NH_2	0.39	−1.32	0.46	−1.33
NH_3	0.16	−1.51	0.05	−1.56
N_2H	0.57	0.21	0.77	0.05
N_2H_2	0.54	0.01	0.66	−0.15
N_2H_3	0.46	−0.25	0.50	−0.28

0.1–0.6 eV for the bulk M12 nanoclusters. For the relaxed M12 nanoclusters the electronic effect is small. Comparing these effects with the previous obtained shifts between close-packed and stepped surfaces the geometrical effect is minor.[61,63]

The fixation of the metals in the M12 structure will, however, influence the calculated adsorption energies and hence effect the determined scaling relations. Structures with or without adsorbates would all have had lower energy, if the structures were allowed to relax fully but this study is focused on determining trends in such under-coordinated structures. Calculations with completely free metal atoms will be difficult to investigate systematically for the examined metals.

In Fig. 4, the scaling relations for the adsorption energy of a N_2 molecule and an H adatom are plotted against the adsorption energy of N adatoms. The slope for the adsorption energies of 0.2 for H adatoms lies close to what previously has been documented in the literature.[35] The scaling relation for a H adatom is systematic and there is only a minor electronic effect between the bulk M12 and the relaxed M12 nanoclusters, see Fig. S5 in the ESI.† The shift between the M12 nanocluster calculations and the fcc(211) stepped calculations for H is again minor and there are no signs of a noticeable geometric effect, see Fig. S6 in the ESI.†

However, for the N_2 scaling relation there is a significant variation in the slope. The bulk M12 nanocluster has a slope of 0.46, while the relaxed M12 nanocluster gives a slope of 0.26, see Fig. S7 in the ESI.† The values for the relaxed M12 correspond very well to the reference calculations on the fcc(211) stepped surface, see Fig. S6 in the ESI,† which gives a slope of 0.31; the slope for N_2 scaling of 0.3 was reported in the literature for both stepped and close-packed surfaces.[61]

The variation in the adsorption energy of N_2 between the bulk M12 and relaxed M12 nanocluster calculations originates from a combination of an electronic effect from the relaxation of the lattice constant, causing a shift along the scaling relation line, and a geometric effect caused by different adsorption geometries for the reactive metals compared to the noble metals. For the reactive metals, the adsorption sites are disigma bonded while for the more noble metals N_2 is adsorbed as an antenna on the surface, which could explain the big change observed specifically for the reactive metals. This difference in adsorption geometry can influence the strength of the adsorption when changing the overall reactivity of the nanocluster going from one M12 lattice constant to another. For the other reaction intermediates studied in this work and N_2 on the noble metals, one nitrogen atom is mainly bound to the surface, while for N_2 on the reactive metals, both nitrogen atoms are adsorbed onto the surface. The adsorption sites for the adsorbed N_2 molecule are different on the stepped fcc(211) surface where the N_2 molecule is bonded to the edge and terrace at the same time.[32,34,35] The consequences of this dramatic change are that the associative mechanism on the bulk M12 nanoclusters seems to be more active. The same tendencies are seen for the other important reaction intermediates NH_3 and N_2H. These three reaction intermediates are key reaction species for the associative mechanism and therefore a shift in scaling relations is very interesting.

In Fig. 5, the linear scaling relations for the N_2H_x adsorbates are shown. In the plot only the adsorption energies calculated for the N_2H, N_2H_2, and N_2H_3 species are included, since adsorbates containing more hydrogen spontaneously split into

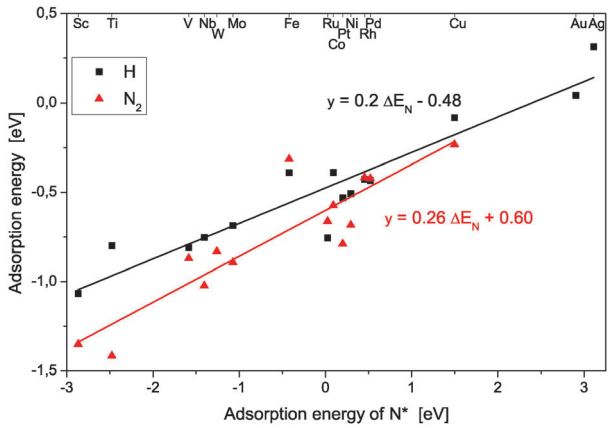

Fig. 4 The scaling relations for N_2 and H species on the M12 nanoclusters consisting of transition metals. The adsorption positions are chosen as the most stable ones.

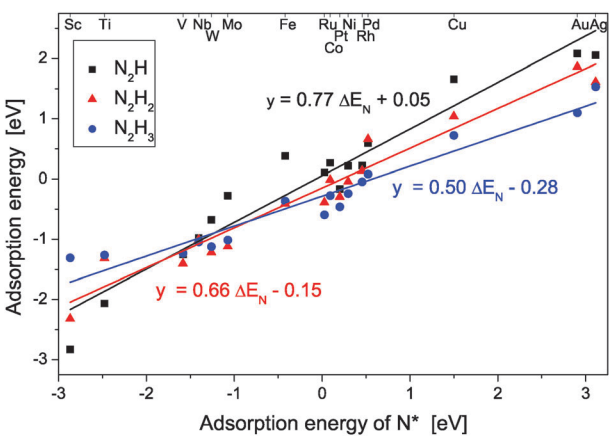

Fig. 5 The scaling relations for N_2H_x species on the M12 nanoclusters consisting of transition metals. The adsorption positions are chosen as the most stable ones.

two molecules, ranging over NH, NH_2, NH_3 to NH_3(g). The slopes for the species are 0.77, 0.66 and 0.50 for N_2H, N_2H_2 and N_2H_3 respectively. The slopes for N_2H and N_2H_2 species are different than those of the reference system of the stepped fcc(211) surface, see Fig. S8 in the ESI.† These relations again present a change in the mechanics for the associative mechanism for the under-coordinated reaction sites. To compare with the substantial effect effects between the bulk M12 and relaxed M12 nanoclusters are observed for N_2, there is no change between the two systems, see Fig. S9–S11 in the ESI,† indicating that the electronic effect on N_2 is higher because the N_2 is bonded to two sites, whereas N_2H_x species are bonded mostly to one site.

The simple underlying argument for scaling relations for AH_x species (where A is N in this case) does not hold for more complicated molecules, such as the A_2H_x molecules considered in this work. The internal bonding of orbitals in the A–A backbone will make a derivation similar to the one carried out for AH_x species much more complicated and may depend more strongly on the local adsorption environment; *i.e.* whether both backbone atoms bind to the surface or only one, and how will the hydrogen atoms bind to one or both backbone atoms and how this may effect the bonding.

C. Entropy and zero point energy corrections

The established linear scaling relations greatly simplify the adsorption energies for all reaction intermediates on all involved metals. As a reference the gas-phase entropy of nitrogen and hydrogen molecules has been used. The conditions for which the corrections have been calculated are ambient conditions, room temperature and 1 bar. The corrections for the zero point energy E_{ZPE} and for the entropy S have been calculated using statistical mechanics for the surface intermediates, see eqn (7) and (8), respectively, and for the gas phase species table values have been used.[64,65]

The calculated thermodynamic corrections are presented in Table 2. These thermodynamic corrections have been calculated for all adsorption species on the Ru M12 nanocluster and have been used as a first order approximation for the entropy and zero point energy terms for the other metals and later tested on Mo. It is reasonable to expect that the difference in the correction terms across the metals is small because the type of adsorption site for each reaction intermediate is similar.

IV. Volcano plots

Using the tools described above, it is possible to create plots visualizing the onset potential for electrochemical nitrogen fixation. This method was introduced in ref. 58 for the electrolysis of water on oxide surfaces.

In this analysis, the reaction free energy can be used directly as a simple measure of electrocatalytic activity. The reaction free energy for each elementary step can be expressed as functions of the applied bias U and the adsorption energy ΔE_N or the reaction free energy ΔG_N of the nitrogen adatom (N*). This is possible because the linear scaling relations

Table 2 The thermodynamic corrections for the reaction intermediates on the M12 nanocluster calculated at 298 K. These corrections are based on statistical thermodynamics calculated using harmonic vibration of adsorbates on the surface

Molecule	ZPE (eV)	TS (eV K^{-1})
Gas-phase		298 K
N_2(g)	0.211	0.592
H_2(g)	0.344	0.404
NH_3(g)	0.985	0.596
M12 nanocluster		298 K
N*	0.076	0.020
H*	0.171	0.014
N_2*	0.182	0.033
NH*	0.365	0.032
NH_2*	0.713	0.041
NH_3*	1.036	0.058
N_2H*	0.480	0.057
N_2H_2*	0.796	0.067
N_2H_3*	1.135	0.063

combined with the approximation that the free energy corrections at the Ru M12 nanocluster describe all important trends for the electrocatalytic activity. All protonation steps for both the *dissociative* and *associative* mechanisms include removal of a proton and an electron from the surrounding electrolyte and addition of a hydrogen to the adsorbed molecule. A dependency on the applied potential will therefore be a direct result of this framework. In the following, the method to determine the onset potential as a function of the free energy of an adsorbed nitrogen adatom will be illustrated.

The free energy of a basic protonation reaction where both reaction intermediates (initial and final state) are bonded to the surface, *e.g.* eqn (3d), can be described solely by the reactants taking active part in the electron transfer. The result is a simplification of the reaction described in eqn (3d) to the following reaction:

$$\begin{aligned} &NH^* + 2(H^+ + e^-) \rightleftharpoons NH_2^* + (H^+ + e^-), \\ &\Delta G_{dis,2} = \Delta G_{NH_2^*} - \Delta G_{NH^*} \end{aligned} \tag{12}$$

which describes the change in free energy of the reaction as defined in eqn (9). Inserting the general expression for the scaling relations formulated in eqn (10) into the equation above, the change in free energy for this part reaction is given as a function of the nitrogen binding energy, ΔE_N, and the applied potential, U.

$$\begin{aligned} \Delta G_{dis,2} &= \Delta G_{NH_2^*} - \Delta G_{NH^*} \\ &= \alpha_{NH_2}\Delta E_N + \kappa_{NH_2} + E_{ZPE,NH_2} - T\Delta S_{NH_2} - eU \\ &\quad - (\alpha_{NH}\Delta E_N) + \kappa_{NH} + E_{ZPE,NH} - T\Delta S_{NH} - 2eU \\ &= (\alpha_{NH_2} - \alpha_{NH})\Delta E_N + eU \\ &\quad + (\kappa_{NH_2} + E_{ZPE,NH_2} - T\Delta S_{NH_2}) \\ &\quad - (\kappa_{NH} + E_{ZPE,NH} - T\Delta S_{NH}). \end{aligned} \tag{13}$$

Inserting the derived numbers from the scaling relations presented in Table 1 and the calculated free energy corrections

from Table 2 into eqn (13) and subsequently converting ΔE_N to ΔG_N yield:

$$\Delta G_{dis,2} = -0.26\Delta E_N - 0.34\ \text{eV} + eU$$
$$= -0.26(\Delta G_N - 0.23\ \text{eV}) - 0.34\ \text{eV} + eU$$
$$= -0.26\Delta G_N - 0.28\ \text{eV} + eU, \quad (14)$$

where 0.23 eV is the calculated change in energy going from adsorption energy to reaction free energy for an adsorbed nitrogen adatom. The next step that must be taken is to apply a potential such that each forward reaction has a negative free energy change and the onset potential is defined when $\Delta G_{dis,2} = 0$. This ensures that the reaction occurs spontaneously, as long as the protonation barrier is low. Applying this constraint to eqn (14), the minimum onset potential needed to drive this specific reaction is given by:

$$U = 0.26/e \times \Delta E_N + 0.28\ \text{V} \quad (15)$$

where e is the elementary charge.

This procedure can be done for all pure protonation steps and plotting the obtained expressions in one plot will form a volcano describing the necessary onset potential which makes each part reaction exothermic. Fig. 6 shows both the associative and dissociative processes. The associative process is purely electrochemical, whereas the dissociative process involves the non-electrochemical (thermal) step, *i.e.* the splitting of the N–N bond, which has to be dealt with separately as outlined below.

The volcano plot for the associative mechanism can be understood utilizing the method behind eqn (13)–(15), and the two solid lines in Fig. 6 form a volcano. These part reactions are the ones that limit the associative electrochemical ammonia synthesis. The two solid lines form a volcano, where the lowest onset potential for driving the associative ammonia synthesis electrochemically is close to $U = -0.45$ V. None of the investigated metals are, however, at the optimal reaction free energy of a nitrogen adatom at −0.5 eV. The closest metals are divided into two groups, one consisting of the more reactive metals Mo, V and Nb and the other group consisting of Fe being by far the closest metal and Ru, Pt and Co further away. Here Ru and Fe are already well known good heterogeneous catalyst materials for the Haber–Bosch process and are unfortunately even better HER catalysts. Finding that the optimum for the associative mechanism lies between Mo and Fe fits very well with the active site in the enzyme nitrogenase which is the iron molybdenum cofactor.[28] Employing this methodology, effects such as coverage dependence, and the dissociation of N_2 or desorption of NH_3 in particular are not included and will have an effect on the predicted efficiency. However, this analysis suggests that alloy particles with free energies of −0.5 eV for adsorbed N adatoms should be good catalysts for the associative mechanism.

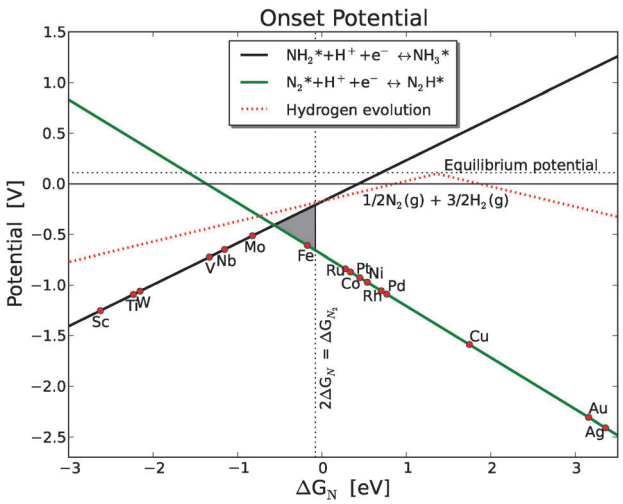

Fig. 6 Volcano plot for the associative and dissociative mechanisms with the free energy ΔG_{N^*} as a descriptor. The competing reaction of creating hydrogen on the surface is also shown as the dotted lines. The two solid lines indicate the limiting potential for the associative mechanism. For the dissociative mechanism the gray area is added as a potential area which could be more favorable for the dissociative mechanism. The efficiency in this area is dependent on the dissociation of the N_2 molecule on the surface. At the top of the gray area the dissociative mechanism will be comparable to HER.

The above-mentioned framework does not describe the main challenges of the dissociative mechanism because it lacks the description of the dissociation of N_2 on the surface. Furthermore, this description will not form one of the two legs to create the volcano (in this case the so-called right leg), see Fig. 6 where the solid black line is the electrochemical limiting reaction for the dissociative mechanism. The reason for this behavior is the scaling relations and that the slopes depend on the number of hydrogen vacancy in the adsorbed molecule. The lines describing the necessary onset potential for the dissociative mechanisms will therefore have slopes with the same sign and almost the same size. The consequence of this behavior will be that the limitations to the electrochemical reaction will only be described for the reactive metals and lack for the noble metals. This description suggests that the electrochemical nitrogen fixation efficiency will be perfect over the noble metals. However, this picture is not correct, since the main hindrance for the noble metals is the N_2 dissociation. The dissociation of N_2 is not affected by the potential and is normally seen as a heterogeneous reaction step and will have activation barriers that is much higher for noble metals than for reactive metals described by the Brøndsted–Evans–Polanyi lines.[60] For the good dissociation catalysts (the reactive metals) the hydrogen evolution reaction is preferred compared to ammonia production. This is the reason why a shift of the volcano utilizing the structure (in)sensitivity to relatively enhance the ammonia production with respect to HER is interesting.

Another method is therefore needed to describe the limitations for the dissociative mechanism on the right leg. Three limitations that should be satisfied for the dissociation of N_2 to be possible on the surfaces are:

(1) It should be preferred to have a nitrogen molecule bonded to the surface. The free energy of N_2* should hence be negative. This break-point is located at $\Delta G_N = 0.03$ eV.

(2) The reaction free energy of $N_2(g)$ to 2N* should be negative and hence exothermic. This corresponds to $\Delta G_N = 0$ eV

and describes the point where the nitrogen atoms are able to bind to the surface.

(3) The gain in reaction free energy for the dissociation reaction of N_2* to 2N* on the surface should be negative, hence leading to a more stable end configuration. Using the linear scaling relations and free energy corrections for both N and N_2, a point can be determined where the gain in free energy for this part reaction is zero. This occurs at the reaction free energy of nitrogen adatoms at −0.08 eV.

The most conservative limit has been implemented as a horizontal line in Fig. 6. Together with the line defining the limiting onset potentials, this limit adds a triangle to the existing associative volcano and this triangle is marked with gray.

These three possible ways of looking at the limiting step for the dissociative mechanism give an estimate of the upper and lower bounds when the dissociative mechanism will be limited by the dissociation. Including one of the other proposed limitations only shift the top of the volcano by 0.11 eV on the *x*-axis and only have a minor change in the onset bias. The added triangle only marks a potential increase in electrocatalytic activity and is to some degree uncertain. Here it is worth noting that in the gray marked area the vertical line is the best case scenario, while the two lines are the worst case.

Comparing the onset potential for ammonia and hydrogen production it is only at the very top of the volcano that there is a possibility of ammonia production requiring a lower onset potential than hydrogen production. As it seems from this volcano it would still be marginally preferred to create hydrogen. However, there will be effects not included in this analysis that will have an effect on the efficiency of the catalyst and on the competition between ammonia and hydrogen production such as coverage, adsorbate–adsorbate effects, the surrounding electrolyte affecting the equilibrium. Furthermore, the fixed geometry used in this study could also influence the results. But it is important to see this study as a trend study to understand to some degree how under-coordinated reactive sites can act as ammonia catalysts.

The volcano plot in Fig. 6 shows the potential determining steps of both the dissociative and associative mechanisms when using the free energy corrections calculated for the adsorbed reaction intermediates within the harmonic approximation. Leaving out the free energy corrections would yield a minor shift for the top of the volcano where the free energy for an adsorbed nitrogen adatom shifts from −0.5 eV to −0.6 eV while the onset potential shifts to 0.4 eV, see Fig. S12 in the ESI.† The potential determining step remains the same for the new volcano and the overall trend is the same, however NH_3 would be favored compared to HER. The fact that the top of the volcano is positioned close to the same free energy of the adsorbed nitrogen adatom indicates that the overall trends for these very under-coordinated reaction sites are to a large degree independent of the calculated free energy corrections.

V. Conclusion

A theoretical analysis of the highly under-coordinated reaction sites of forming ammonia electrochemically on pure transition metal electrodes indicates that the associative mechanism could yield ammonia at an onset potential around −0.6 to −0.45 V with respect to SHE. Here, the hydrogen reaction will be a competing reaction and have a slightly lower onset potential and hence should be preferred. The most promising candidate for electrochemical ammonia production through the associative mechanism is Mo but closely followed by Fe. Alloy materials with reactivities between that of Mo, Fe and Ru could also be candidates, especially if they can hinder the HER and still be good catalysts for NH_3 production. Additionally, alloys with a reactivity such that the free energy of N adsorbed onto the surface is in the vicinity of −0.5 eV. However, even for these very under-coordinated structures there is still a gap between HER and electrochemical ammonia production in terms of onset potential for the potential determining steps. Though this problem could potentially be solved by further utilizing the structure (in)sensitivity, this remains the main challenge for the electrochemical ammonia production.

For the dissociative mechanism a proposed onset potential of −0.5 to −0.1 could be obtained with a preferred ammonia production with respect to HER for the potential determining steps. However, for the dissociative mechanism N_2 dissociation barrier of splitting the N_2 molecule has not been included since this would require a purely thermally activated Langmuir-type mechanism for one elementary step combined with the electrochemical onset potential. Instead an estimate of the equilibrium of having N adatoms compared to N_2 molecules on the surface has been established and this will hence act as a cut-off for the noble metals and describe to some extent the limitations for these metals for the dissociation of a nitrogen molecule on the surface. The cutoff could vary depending on the detailed treatment from a free energy of N adatoms of −0.08 eV to 0.03 eV, which gives the overall uncertainty of approximately 0.1 V in onset potential for the potential determining steps.

Acknowledgements

The authors would like to acknowledge the Danish Center for Scientific Computing for supercomputer access. The Center for Atomic-scale Material Design (CAMD) and the Catalysis for Sustainable Energy (CASE) initiative is funded by the Danish Ministry of Science, Technology and Innovation. This work was funded in part by the U.S. Department of Energy under contract number DE-AC02-76SF00515.

References

1 V. Smil, Detonator of the population explosion, *Nature*, 1999, **400**, 415.
2 V. Smil, *Enriching the earth: Fritz Haber, Carl Bosch, and the Transformation of World Food Production*, Massachusetts Institute of Technology, 2001.
3 A. Klerke, C. H. Christensen, J. K. Nørskov and T. Vegge, Ammonia for hydrogen storage: challenges and opportunities, *J. Mater. Chem.*, 2008, **18**(20), 2304–2310.
4 D. R. Lide, *CRC Handbook of Chemistry and Physics*, CRC Press, 90th edn, 2009.

5 F. Haber and G. van Oordt, Über die Bildung von Ammoniak aus den Elementen, *Z. Anorg. Chem.*, 1905, **47**, 42–44.
6 L. Stryer, *Biochemistry*, W.H. Freeman, New York, 4th edn, 1995.
7 G. Ertl, Z. Paal and S. B. Lee, Structure sensitivity in the iron single-crystal catalyzed synthesis of ammonia, *Appl. Surf. Sci.*, 1981, **8**, 231–249.
8 G. Ertl, M. Weiss and S. B. Lee, Role of potassium in the catalytic synthesis of ammonia, *Chem. Phys. Lett.*, 1979, **60**, 391–394.
9 N. D. Spencer, R. C. Schoonmaker and G. A. Somorjai, Structure sensitivity in the iron single-crystal catalyzed synthesis of ammonia, *Nature*, 1981, **294**, 643–644.
10 G. Ertl, S. B. Lee and M. Weiss, Kinetics of nitrogen adsorption on fe(111), *Surf. Sci.*, 1982, **114**, 515–526.
11 G. Ertl, S. B. Lee and M. Weiss, Adsorption of nitrogen on potassium promoted fe(111) and (100) surfaces, *Surf. Sci.*, 1982, **114**, 527–545.
12 N. D. Spencer, R. C. Schoonmaker and G. A. Somorjai, Iron single crystals as ammonia synthesis catalysts: effect of surface-structure on catalyst activity, *J. Catal.*, 1982, **74**, 129–135.
13 G. Ertl, Primary steps in catalytic synthesis of ammonia, *J. Vac. Sci. Technol., A*, 1983, **1**, 1247–1253.
14 L. Volpe and M. Boudart, Ammonia synthesis on molybdenum nitride, *J. Phys. Chem.*, 1986, **90**, 4874–4877.
15 D. R. Strongin, J. Carrazza, S. R. Bare and G. A. Somorjai, The importance of C7 sites and surface-roughness in the ammonia synthesis reaction over iron, *J. Catal.*, 1987, **103**, 213–215.
16 D. R. Strongin and G. A. Somorjai, The effects of potassium on ammonia synthesis over iron single-crystal surfaces, *J. Catal.*, 1988, **109**, 51–60.
17 J. A. Dumesic and A. A. Trevino, Kinetic simulation of ammonia synthesis catalysis, *J. Catal.*, 1989, **116**, 119–129.
18 L. M. Aparicio and J. A. Dumesic, Ammonia synthesis kinetics: surface chemistry, rate expressions, and kinetic analysis, *J. Mater. Chem.*, 2008, **18**, 2304–2310.
19 M. Boudart, Ammonia synthesis: the bellwether reaction in heterogeneous catalysis, *Top. Catal.*, 1994, **1**, 405–414.
20 A. Nielsen, *Ammonia: catalysis and manufacture*, Springer-Verlag, 1995.
21 G. Marnellos and M. Stoukides, Ammonia synthesis at atmospheric pressure, *J. Mater. Chem.*, 1988, **282**, 98–100.
22 S. Dahl, A. Logadottir, R. C. Egeberg, J. H. Larsen, I. Chorkendorff, E. Törnqvist and J. K. Nørskov, Role of steps in N2 activation on Ru(0001), *Phys. Rev. Lett.*, 1999, **83**, 1814–1817.
23 S. Dahl, E. Törnqvist and I. Chorkendorff, Dissociative adsorption of N2 on Ru(0001): a surface reaction totally dominated by steps, *J. Catal.*, 2000, **192**, 381–390.
24 S. Dahl, J. Sehested, C. J. H. Jacobsen, E. Törnqvist and I. Chorkendorff, Surface science based microkinetic analysis of ammonia synthesis over ruthenium catalysts, *J. Catal.*, 2000, **192**, 391–399.
25 T. Murakami, T. Nishikiori, T. Nohira and Y. Ito, Electrolytic synthesis of ammonia in molten salts under atmospheric pressure, *J. Am. Chem. Soc.*, 2003, **125**, 334–335.
26 R. Kojima and K. Aika, Molybdenum nitride and carbide catalysts for ammonia synthesis, *Appl. Catal., A*, 2001, **219**, 141–147.
27 T. H. Rod, A. Logadottir and J. K. Nørskov, Ammonia synthesis at low temperatures, *J. Chem. Phys.*, 2000, **112**, 5343–5347.
28 B. Hinnemann and J. K. Nørskov, Modeling a central ligand in the nitrogenase femo cofactor, *J. Am. Chem. Soc.*, 2003, **125**, 1466–1467.
29 A. Logadottir, T. H. Rod, J. K. Nørskov, B. Hammer, S. Dahl and C. J. H. Jacobsen, The Brønsted–Evans–Polanyi Relation and the Volcano Plot for Ammonia Synthesis over Transition Metal Catalysts, *J. Catal.*, 2001, **197**(2), 229–231.
30 A. Logadottir and J. K. Nørskov, Ammonia synthesis over a Ru(0001) surface studied by density functional calculations, *J. Catal.*, 2003, **220**, 273–279.
31 A. Hellman, K. Honkala, I. N. Remediakis, A. Logadottir, A. Carlsson, S. Dahl, C. H. Christensen and J. K. Nørskov, Ammonia synthesis and decomposition on a ru-based catalyst modeled by first-principles, *Surf. Sci.*, 2009, **603**, 1731–1739.
32 A. Hellman, E. J. Baerends, M. Biczysko, T. Bligaard, C. H. Christensen, D. C. Clary, S. Dahl, R. van Harrevelt, K. Honkala, H. Jónsson, G. J. Kroes, M. Luppi, U. Manthe, J. K. Nørskov, R. A. Olsen, J. Rossmeisl, E. Skulason, C. S. Tautermann, A. J. C. Varandas and J. K. Vincent, Predicting catalysis: understanding ammonia synthesis from first-principles calculations, *J. Phys. Chem. B*, 2006, **110**, 17719–17735.
33 T. Song and P. Hu, Insight into the adsorption competition and the relationship between dissociation and association reactions in ammonia synthesis, *J. Chem. Phys.*, 2007, **127**, 234706.
34 K. Honkala, A. Hellman, I. N. Remediakis, A. Logadottir, A. Carlsson, S. Dahl, C. H. Christensen and J. K. Nørskov, Ammonia synthesis from first-principles calculations, *Science*, 2005, **307**, 555–558.
35 E. Skúlason, T. Bligaard, S. Gudmundsdottir, F. Studt, J. Rossmeisl, F. Abild-Pedersen, T. Vegge, H. Jónsson and J. K. Nørskov, A theoretical evaluation of possible transition metal electro-catalysts for N_2 reduction, *Phys. Chem. Chem. Phys.*, 2012, **14**, 1235–1245.
36 C. J. H. Jacobsen, S. Dahl, P. L. Hansen, E. Törnqvist, L. Jensen, H. Topsoe, D. V. Prip, P. B. Moenshaug and I. Chorkendorff, Structure sensitivity of supported ruthenium catalysts for ammonia synthesis, *J. Mol. Catal. A: Chem.*, 2000, **163**, 19–26.
37 R. Gomez, A. Fernandez-Vega, J. M. Feliu and A. Aldaz, Hydrogen evolution on platinum single crystal surfaces: effects of irreversibly adsorbed bismuth and antimony on hydrogen adsorption and evolution on platinum (100), *J. Phys. Chem.*, 1993, **97**(18), 4769–4776.
38 M. Haruta, S. Tsubota, T. Kobayashi, H. Kageyama, M. J. Genet and B. Delmon, Low-Temperature Oxidation

of CO over Gold Supported on TiO_2, α-Fe_2O_3, and Co_3O_4, *J. Catal.*, 1993, **144**, 175–192.

39 J. Kleis, J. Greeley, N. A. Romero, V. A. Morozov, H. Falsig, A. H. Larsen, J. Lu, J. J. Mortensen, M. Dułak, K. S. Thygesen, J. K. Nørskov and K. W. Jacobsen, Finite Size Effects in Chemical Bonding: from Small Clusters to Solids, *Catal. Lett.*, 2011, **141**, 1067–1071.

40 T. Jiang, D. J. Mowbray, S. Dobrin, H. Falsig, B. Hvolbaek, T. Bligaard and J. K. Nørskov, Trends in co oxidation rates for metal nanoparticles and close-packed, stepped, and kinked surfaces, *J. Phys. Chem. C*, 2009, **113**, 10548.

41 J. K. Nørskov, T. Bligaard, J. Rossmeisl and C. H. Christensen, Towards the computational design of solid catalysts, *Nat. Chem.*, 2009, **1**, 37–46.

42 P. Hohenberg and W. Kohn, Inhomogeneous electron gas, *Phys. Rev. B: Solid State*, 1964, **136**(3), B864–B871.

43 W. Kohn and L. J. Sham, Self-consistent equations including exchange and correlation effects, *Phys. Rev. Sect. A*, 1965, **140**(4), A1133–A1138.

44 B. Hammer, L. B. Hansen and J. K. Nørskov, Improved adsorption energetics within density-functional theory using revised Perdew-Burke-Ernzerhof functionals, *Phys. Rev.*, 1999, **59**(11), 7413–7421.

45 P. E. Blöchl, C. J. Först and J. Schimpl, Projector augmented wave method: *ab-initio* molecular dynamics with full wave functions, *Bull. Mater. Sci.*, 2003, **26**, 33.

46 P. E. Blöchl, Projector Augmented Wave Method, *Phys. Rev. B: Condens. Matter Mater. Phys.*, 1994, **50**(24), 17953–17979.

47 J. J. Mortensen, L. B. Hansen and K. W. Jacobsen, Real-space grid implementation of the projector augmented wave method, *Phys. Rev. B: Condens. Matter Mater. Phys.*, 2005, **71**, 33.

48 J. J. Mortensen, *et al.*, Electronic structure calculations with gpaw: a real-space implementation of the projector augmented-wave method, *J. Phys.: Condens. Matter*, 2010, **22**, 253202.

49 The GPAW code is available as a part of the CAMPOS software: http://www.camd.dtu.dk/Software.

50 H. J. Monkhorst and J. D. Pack, Special points for brillouin-zone integrations, *Phys. Rev. B: Solid State*, 1976, **13**(12), 5188–5192.

51 The ASE code is available as a part of the CAMPOS software: http://www.camd.dtu.dk/Software.

52 J. Heyrovski, A theory of overpotential, *Recl. Trav. Chim. Pays-Bas*, 1927, **46**(8), 582–585.

53 S. Wang, V. Petzold, V. Tripkovic, J. Kleis, J. G. Howalt, E. Skulason, E. M. Fernandez, B. Hvolbaek, G. Jones, A. Toftelund, H. Falsig, M. Björketun, F. Studt, F. Abild-Pedersen, J. Rossmeisl, J. K. Nørskov and T. Bligaard, Universal transition state scaling relations for (de)hydrogenation over transition metals, *Phys. Chem. Chem. Phys.*, 2011, **13**(46), 20760–20765.

54 J. Tafel, On the polarization during cathodic hydrogen evolution, *Z. Phys. Chem.*, 1905, **50**, 641.

55 T. Vegge, T. Rasmussen, T. Leffers, O. B. Pedersen and K. W. Jacobsen, Atomistic simulations of cross-slip of jogged screw dislocations in copper, *Philos. Mag. Lett.*, 2001, **81**, 137–144.

56 J. K. Nørskov, J. Rossmeisl, A. Logadottir, L. Lindqvist, J. R. Kitchin, T. Bligaard and H. Jónsson, Origin of the overpotential for oxygen reduction at a fuel-cell cathode, *J. Phys. Chem. B*, 2004, **108**(46), 17886–17892.

57 J. Rossmeisl, A. Logadottir and J. K. Nørskov, Electrolysis of water on (oxidized) metal surfaces, *Chem. Phys.*, 2005, **319**, 178–184.

58 J. Rossmeisl, Z.-W. Qu, G.-J. Kroes and J. K. Nørskov, Electrolysis of water on oxide surfaces, *J. Electroanal. Chem.*, 2007, **607**, 83–89.

59 A. A. Peterson, F. Abild-Pedersen, F. Studt, J. Rossmeisl and J. K. Nørskov, How copper catalyzes the electroreduction of carbon dioxide into hydrocarbon fuels, *Energy Environ. Sci.*, 2010, **3**, 1311–1315.

60 S. G. Wang, B. Temel, J. A. Shen, G. Jones, L. C. Grabow, F. Studt, T. Bligaard, F. Abild-Pedersen, C. H. Christensen and J. K. Nørskov, Universal Brønsted-Evans-Polanyi Relations for C–C, C–O, C–N, N–O, N–N, and O–O Dissociation Reactions, *Catal. Lett.*, 2011, 141.

61 F. Abild-Petersen, J. Greeley, F. Studt, J. Rossmeisl, T. R. Munter, P. G. Moses, E. Skulason, T. Bligaard and J. K. Nørskov, Scaling properties of adsorption enemies for hydrogen containing molecules on transition metal surfaces, *Phys. Rev. Lett.*, 2007, **99**, 016105–016108.

62 M. Mavrikakis, B. Hammer and J. K. Nørskov, Effect of Strain on the Reactivity of Metal Surfaces, *Phys. Rev. Lett.*, 1998, **81**(13), 2819–2822.

63 J. K. Nørskov, T. Bligaard, B. Hvolbæk, F. Abild-Pedersen, I. Chorkendorff and C. H. Christensen, The nature of the active site in heterogeneous metal catalysis, *Chem. Soc. Rev.*, 2008, **37**, 2163–2171.

64 R. J. Silbey, R. A. Alberty and M. G. Bawendi, *Physical Chemistry*, Wiley, 4th edn, 2005.

65 C. J. Cramer, *Physical Chemistry*, John Wiley & Sons, Ltd., 2nd edn, 2004.